High-Power Narrow-Band Terahertz Generation Using Large-Aperture Photoconductors

Sang-Gyu Park, *Member, IEEE,* A. M. Weiner, *Fellow, IEEE,* Michael R. Melloch, *Fellow, IEEE,* Craig W. Siders, Jennifer L. W. Siders, and Antoinette J. Taylor

***Abstract*— Large-aperture biased photoconductive emitters which can generate high-power narrow-band terahertz (THz) radiation are developed. These emitters avoid saturation at high fluence excitation and achieve enhanced peak power spectral density by employing a thick layer of short-lifetime low-temperature-grown GaAs (LT-GaAs) photoconductor and multiple-pulse excitation. THz waveforms are calculated from the saturation theory of large-aperture photoconductors, and a comparison is made between theory and measurement. A direct comparison of the multiple-pulse saturation properties of THz emission from semi-insulating GaAs and LT-GaAs emitters reveals a strong dependence on the carrier lifetime. In particular, the data demonstrate that saturation is avoided only when the interpulse spacing is longer than the carrier lifetime.**

***Index Terms*— Large-aperture, low-temperature-grown GaAs, photoconductor, saturation, terahertz.**

I. Introduction

TERAHERTZ (THz) radiation has been the focus of intense research for over a decade. THz radiation has been generated by illuminating various emitters, including externally biased photoconductive (PC) antennas, surface built-in field biased semiconductors, and nonlinear crystals with short optical pulses. The strongest radiative power below 2 THz has been generated by externally biased PC antennas [1]–[3]. High-power THz radiation is desirable for a number of applications both in science and engineering. Therefore, a great deal of effort has been made to understand the limitations of the available emitters and to increase the power of emitted THz radiation [1]–[8].

The generation of narrow-band THz radiation was demonstrated by Liu *et al.* [9], [10] and Weling *et al.* [11], in which PC emitters were excited using optical pulse trains derived from femtosecond optical pulse-shaping [9], [10] or interference of highly chirped optical pulses [11]. Such narrow-band THz radiation can be applied to communications or spectroscopy where narrow-band excitation and/or tunability is desirable. For nonlinear spectroscopy, high-power radiation as well as narrow-band THz radiation is also desirable. Liu *et al.* demonstrated that, by using multiple-pulse excitation, one can avoid saturation of the THz emitter and generate a larger peak power at the selected THz frequency compared to single-pulse excitation [9]. The work of Liu *et al.* and Weling *et al.* was performed with dipole antenna emitters and weak (<1 nJ) excitation pulses. For high-power THz radiation, the use of large-aperture antennas and high-energy pulse excitation is recommended.

In this paper, we present our investigations on high-power narrow-band THz large-aperture PC emitters [12]. We have developed large-aperture PC antennas for narrow-band THz radiation that can be used with amplified excitation pulses with fluences of up to several mJ/cm^2. We significantly reduced saturation effects and substantially enhanced the peak power spectral density of the emitted THz radiation by using multiple-pulse excitation of PC emitters fabricated on a low-temperature-grown gallium arsenide (LT-GaAs) photoconductor [13], [14]. Because of the near-field nature of the field-screening of the biased emitter, we find that short carrier lifetime of the photoconductor is very important. We also determined that the thickness of the short carrier lifetime photoconductor is important when designing emitters for use with high excitation fluence. When the thin-film photoconductor is excited by high fluence optical pulses, a portion of light penetrates into the substrate which has a long carrier lifetime, which in turn degrades the performance of the PC emitter.

In Section II, we review the theory of saturation of large-aperture PC antennas and discuss important factors in the design of large-aperture PC emitters. The modeling procedure which we developed to predict THz radiation from the antenna will also be presented. We describe the experimental setup in Section III. In Section IV, experimental results will be discussed, and in Section V we conclude.

II. Design of the Large-Aperture PC-Antenna for High-Power Narrow-Band THz Generation

A. The Theory of Saturation of Large-Aperture Photoconductors

In this section, we review the theory of large-aperture PC antennas and point out important implications. When a large-

Manuscript received January 4, 1999; revised April 15, 1999. The work of S.-G. Park and A. M. Weiner was supported by the National Science Foundation under Grant 9404677-PHY and Grant 9722668-PHY. The work of M. R. Melloch was supported by the Air Force Office of Scientific Research under Grant F49620-96-0234A.

S.-G. Park was with the School of Electrical and Computer Engineering, Purdue University, West Lafayette, IN 47907 USA. He is now with AT&T Labs-Research, Red Bank, NJ 07701 USA.

A. M. Weiner and M. R. Melloch are with the School of Electrical and Computer Engineering, Purdue University, West Lafayette, IN 47907 USA.

C. W. Siders was with Los Alamos National Laboratory, Los Alamos, NM 87545 USA. He is now with the Department of Chemistry and Biochemistry, University of California San Diego, La Jolla, CA 92093 USA.

J. L. W. Siders was with Los Alamos National Laboratory, Los Alamos, NM 87545 USA. She is now with the Department of Physics, University of San Diego, San Diego, CA 92110–2492 USA.

A. J. Taylor is with Los Alamos National Laboratory, Los Alamos, NM 87545 USA.

Publisher Item Identifier S 0018-9197(99)05958-8.

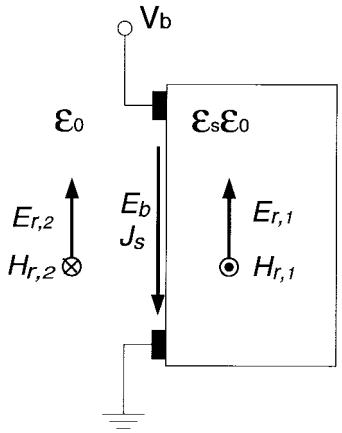

Fig. 1. The photoconductive biased emitter. E_b: biased electric field; V_b: applied voltage; J_s: induced current; $E_{r,1}$, $H_{r,1}$: radiated electric and magnetic field into the semiconductor; and $E_{r,2}$, $H_{r,2}$: radiated electric and magnetic field into the free space.

aperture PC antenna is excited by strong optical pulses, the THz output strength is saturated. This saturation comes from the screening of the externally applied bias field. The origins of this screening are known to be radiation field screening [1] and space-charge screening [5], [15]. In radiation field screening, the near-field generated at the surface by the transient current cancels out a portion of the bias field. For a large-aperture antenna, where the aperture size is larger than the center wavelength of the emitted THz radiation, the radiation field screening effect can be derived from simple electromagnetic boundary conditions as follows [1].

The electric and magnetic fields around the antenna can be divided into stationary fields from the applied bias (E_b, H_b) and transient fields from the induced current from optical excitation (E_r, H_r). Fig. 1 shows a large-aperture PC emitter and depicts the quantities which are relevant to the theory. We use ($E_{r,1}$, $H_{r,1}$) and ($E_{r,2}$, $H_{r,2}$) to designate the transient field inside the semiconductor and free space, respectively. Since there is no current without optical excitation of the emitter, only an electric field E_b is present ($H_b = 0$) before the arrival of the excitation pulses. When the photoconductor is excited, the photogenerated carriers flow in the bias field, generating surface current J_s. When there is surface current density $J_s(t)$, the following boundary conditions hold:

$$E_{r,1}(t) = E_{r,2}(t) \equiv E_r(t) \tag{1}$$

$$J_s(t) = H_{r,2}(t) - H_{r,1}(t). \tag{2}$$

When the aperture of the antenna is large compared to the wavelength of the radiation, $H_{r,2}(t)$ and $H_{r,1}(t)$ can be related to $E_{r,2}(t)$ and $E_{r,1}(t)$ by (3) and (4), respectively,

$$H_{r,1}(t) = \frac{\sqrt{\epsilon_s}}{\eta_0} E_{r,1}(t) \tag{3}$$

$$H_{r,2}(t) = \frac{1}{\eta_0} E_{r,2}(t) \tag{4}$$

where η_0 is the intrinsic impedance of free space and ϵ_s is the relative dielectric constant of the photoconductor. By combining (1)–(4), we obtain the following equation, which relates the surface current to the radiated electric field:

$$E_r(t) = -\frac{\eta_0}{1+\sqrt{\epsilon_s}} J_s(t). \tag{5}$$

Equation (5) tells us that the electric field component developed at the surface by surface current is opposite to the direction of J_s. Also, J_s can be expressed using Ohm's law

$$J_s(t) = \sigma(t)(E_b + E_r(t)) \tag{6}$$

where $\sigma(t)$ is the surface conductivity of the emitting antenna. Combining (5) and (6), we get the following equation for surface current $J_s(t)$:

$$J_s(t) = \frac{\sigma(t) E_b}{1 + \dfrac{\sigma(t)\eta_0}{1+\sqrt{\epsilon_s}}}. \tag{7}$$

It is evident from (7) that the magnitude of the induced current is saturated when $\sigma(t)\eta_0/(1+\sqrt{\epsilon_s}) \geq 1$ (i.e., when excited by high fluence pulses). The far-field radiation $E_{\rm rad}(t)$ from the current distribution $J_s(t)$ on the propagating axis of the radiation can be expressed by [16]

$$E_{\rm rad}(t) \cong -\frac{A}{4\pi\epsilon_0 c^2 r} \frac{dJ_s(t)}{dt} \tag{8}$$

where A is the area of the emitter carrying the current distribution. When comparing (5) and (6), we observe a difference between the far-field and the near-field. The far-field is proportional to the time-derivative of the current, while the near-field is directly proportional to the current. The saturation behavior of the photoconductive emitter is governed by the near-field as shown in (7). Because the near-field is proportional to the surface current, and not to its time-derivative, the saturation effect persists as long as there is current. The difference is clear when a long carrier lifetime photoconductor is considered. When the photoconductor is illuminated by a short optical pulse, a current surge is generated which leads to THz radiation. If the carrier lifetime is long, current keeps flowing long after the excitation pulse is gone. If another pulse arrives before the current dies out and excites the emitter, a new THz pulse will be generated, but this time the background current which is already present may affect the THz generation.

The space-charge screening arises from the separation of the photogenerated electrons and holes in the bias electric field. When the electrons and holes drift in the opposite direction, regions of net positive and negative space charge develop. The electric field induced by this space charge is in the opposite direction to the bias field and screens the bias field. This space screening can be important for small dipole antennas, but, for large-aperture antennas, radiation screening is the major source of the saturation [17].

B. Design Considerations in Developing the Large-Aperture Antenna for Multiple-Pulse Excitation

When designing THz emitters which overcome saturation and generate strong narrow-band radiation, we should consider several things. First, from the near-field nature of the screening, we know that the lifetime of the carrier should be short

compared to the interpulse spacing of the excitation pulse train. Assuming exponential decay, the interpulse spacing should be larger than the lifetime by a factor of two to three in order to reduce the carrier population to below 10% of the peak value. This means that, in order to have narrow-band radiation around 300 GHz, where interpulse spacing is 3.3 ps, a carrier lifetime shorter than 1 ps is required. Another important factor is the thickness of the photoconductive layer. Generally, a fast photoconductive layer is epitaxially grown on another semiconductor substrate with a long carrier lifetime (typically >100 ps). If the excitation pulse penetrates into the substrate, very slowly decaying electron and hole populations are generated, and the performance of the emitter is degraded. For a GaAs epitaxial layer, the absorption coefficient at 800-nm wavelength is $\alpha^{-1} \sim 1$ μm [18]. Therefore, if the thickness of the epitaxial layer is 1 μm, about 30% of the light is absorbed into the substrate. In order to reduce substrate absorption below 5%, at least 3 μm of the epitaxial thickness is required.

Now we will examine the power/amplitude scaling relations of the THz radiation relevant to our work on multiple-pulse excitation. First we examine the case when the THz emitter operates in a linear regime. The optical excitation $I_1(t)$ generates THz radiation $E_1(t)$. Then, the optical excitation is split without loss into N pulses with interpulse separation T as

$$I_N(t) = \frac{1}{N} \sum_{n=0}^{N-1} I_1(t - nT). \tag{9}$$

Since the emitter is in the linear regime, the THz radiation from the N-pulse excitation can be calculated as a linear combination of single-pulse responses shown by

$$E_N(t) = \frac{1}{N} \sum_{n=0}^{N-1} E_1(t - nT). \tag{10}$$

The Fourier spectrum of $E_N(t)$ is given in (14)

$$S_N(\omega) = \int dt\, e^{-i\omega t} E_N(t) \tag{11}$$

$$= \frac{1}{N} \sum_{n=0}^{N-1} e^{i\omega nT} \int dt\, e^{-i\omega t} E_1(t) \tag{12}$$

$$= \frac{1}{N} \frac{1 - e^{Ni\omega T}}{1 - e^{i\omega T}} S_1(\omega) \tag{13}$$

$$= \exp\left[\frac{(N-1)i\omega T}{2}\right] \frac{\mathrm{sinc}(N\omega T/2\pi)}{\mathrm{sinc}(\omega T/2\pi)} S_1(\omega) \tag{14}$$

where $S_1(\omega) = \int dt\, e^{-i\omega t} E_1(t)$ is the Fourier transform of the THz pulse from single-pulse excitation. We now have the multipulse THz spectrum which is represented by the multiplication of the single-pulse THz spectrum and the interference term. As the frequency ω approaches the multiples of the repetition rate of the pulse train, $\omega \to 2\pi m/T$, where m is an integer, and the interference term approaches 1 as shown by

$$\lim_{\omega \to 2\pi m/T} \frac{1}{N} \frac{1 - e^{Ni\omega T}}{1 - e^{i\omega T}} \to 1. \tag{15}$$

When the emitter operates in the linear regime, multiple-pulse excitation of the same integrated optical fluence generates the same peak spectral amplitude as single-pulse excitation at the frequency of $\omega = 2\pi m/T$. There is no gain in terms of the spectral amplitude when we excite the linear emitter with multiple pulses, but the spectrum of the multiple-pulse excited THz becomes narrower as the number of pulses is increased. Therefore, if the purpose of the multiple-pulse excitation is frequency selection, this can be achieved as demonstrated by Liu *et al.* [9], [10].

Now consider the case when the emitter is completely saturated both by a single pulse of $I_1(t)$ and by individual pulses $I_1(t)/N$ of the N-pulse train. Here we consider an ideal situation where the emitter recovers from the saturation very rapidly compared to the interpulse spacing of the multiple-pulse train. Since the emitter is completely saturated, $I_1(t)$ and $I_1(t)/N$ should generate roughly the same THz radiation. In this case, the THz radiation from multiple-pulse excitation is represented by

$$E_N(t) = \sum_{n=0}^{N-1} E_1(t - nT) \tag{16}$$

and the Fourier spectrum $S_N(\omega)$ is given as

$$S_N(\omega) = \frac{1 - e^{Ni\omega T}}{1 - e^{i\omega T}} S_1(\omega). \tag{17}$$

Again, $S_1(\omega)$ is the Fourier transform of the THz generated by single-pulse excitation. At the frequency $\omega = 2\pi m/T$, the spectral amplitude of S_N is N times larger than that of S_1, i.e., $S_N(\omega = 2\pi m/T) = N \times S_1(\omega = 2\pi m/T)$. This translates into an N^2 enhancement in the peak power spectral density of the THz radiation generated by N-pulse excitation, illuminating a completely saturated emitter. The total THz power around $\omega = 2\pi m/T$ is proportional to N since the spectral narrowing partially compensates for the N^2 enhancement in the power density.

When there is partial saturation in the THz output for single-pulse excitation, but still fast interpulse recovery,

$$E_N(t) = \beta \sum_{n=0}^{N-1} E_1(t - nT) \tag{18}$$

where $1/N < \beta < 1$. There will still be enhancement—but reduced—compared to complete saturation.

C. Simulation of THz Radiation from Large-Aperture PC Antennas Subject to Saturation

Numerical calculations were performed to predict the saturation behavior of the emitters quantitatively. We calculated far-field radiation from the large-aperture PC antenna taking into account the saturation. In this calculation, only radiation screening was included. The space-charge screening effect was not considered since it has a negligible effect on the large-aperture antenna [17]. To account for the absorption of the light in the substrate, we used two layers of electrons which correspond to the electrons in the epitaxial thin film and the substrate, respectively. For SI-GaAs emitters, the two

layers were assumed to have the same mobility and the same recombination time.

The electron concentration $n(x, t)$ in the epitaxial layer can be calculated from

$$\frac{\partial n(x,t)}{\partial t} = -\frac{(1-R)}{h\nu}\frac{\partial I_{\rm opt}(x,t)}{\partial x} - \frac{n(x,t)}{\tau_{r,\,\rm epi}} \tag{19}$$

where $\tau_{r,\,\rm epi}$ is the recombination/trap lifetime in the epitaxial layer, $I_{\rm opt}(x, t)$ is the excitation pulse intensity profile, R is the reflection coefficient at the photoconductor surface, x is the distance from the semiconductor surface, and $h\nu$ is the excitation photon energy. In (19), the first term on the right-hand side represents the absorption of the light which leads to the generation of electrons (and holes). The second term represents the removal of electrons from the conduction band through recombination or trapping. The sheet electron concentration in the epitaxial layer is defined as

$$n_{\rm epi}(t) \equiv \int_0^l n(x,t)\,dx \tag{20}$$

where l is the thickness of the epitaxial layer. Then, (19) can be integrated to yield

$$\frac{\partial n_{\rm epi}(t)}{\partial t} = \frac{(1-R)}{h\nu}\{I_{\rm opt}(0,t) - I_{\rm opt}(l,t)\} - \frac{n_{\rm epi}(t)}{\tau_{r,\,\rm epi}} \tag{21}$$

$$= \frac{(1-R)}{h\nu} I_{\rm opt}(0,t)\{1 - e^{-\alpha l}\} - \frac{n_{\rm epi}(t)}{\tau_{r,\,\rm epi}}. \tag{22}$$

In (22), the linear absorption of light with absorption coefficient α was assumed. The sheet electron density in the substrate $n_{\rm sub}(t) \equiv \int_l^\infty n(x,t)\,dx$ is calculated as

$$\frac{\partial n_{\rm sub}(t)}{\partial t} = \frac{(1-R)}{h\nu} I_{\rm opt}(l,t) - \frac{n_{\rm sub}(t)}{\tau_{r,\,\rm sub}} \tag{23}$$

$$= \frac{(1-R)}{h\nu} I_{\rm opt}(0,t) e^{-\alpha l} - \frac{n_{\rm sub}(t)}{\tau_{r,\,\rm sub}} \tag{24}$$

where $\tau_{r,\,\rm sub}$ is the recombination/trap lifetime of electrons in the substrate. In (23) and (24), we assumed that all the light that reaches the substrate will be absorbed inside the substrate and generate electrons and holes.

In (22) and (24), the current transport effect was ignored ($\nabla \cdot J = 0$), since this effect is very small compared to the fast decaying term. The current transport term can approximated by $v(n/L)$, where L is the size of the emitter and v is the velocity of electrons, while the decaying term is n/τ_r. If we use the saturation velocity of GaAs ($v = 10^7$ cm/s), $L = 0.5$ cm, and $\tau_r = 1$ ps, then $(v/L):(1/\tau_r) = 1:(5 \times 10^4)$. Therefore, the current transport term can be safely ignored for the large-aperture antenna calculation.

The surface current density J_s is obtained using (7) with the sheet conductivity given by

$$\sigma(t) = e\mu_{\rm epi} n_{\rm epi}(t) + e\mu_{\rm sub} n_{\rm sub}(t) \tag{25}$$

where $\mu_{\rm epi}$ and $\mu_{\rm sub}$ are time-independent electron mobilities in the epitaxial layer and the substrate, respectively. In this formalism, we ignored the hole concentration due to its low mobility. When we have the surface current $J_s(t)$, we can calculate the far-field radiation $E_{\rm rad}(t)$ using (8).

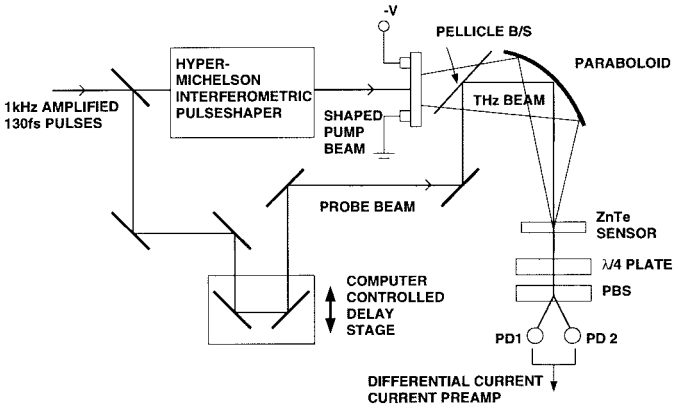

Fig. 2. The schematic of the setup for multiple-pulse excitation experimental.

In order to compare with the measured waveforms, we calculated the waveforms $E_{\rm meas}(t)$ which would be measured from the THz electric field $E_{\rm rad}(t)$. For measuring the THz waveforms, we choose the electrooptic (E-O) sampling technique [19] because of its large bandwidth. In the calculation of the measured waveforms, we took into account the effect of the probe beam pulsewidth $t_{\rm probe}$ and the group velocity mismatch (GVM) of the optical probe and the THz radiation. The GVM effect is important because of the thick (1-mm) sensor ZnTe crystal we used. The optical probe profile with GVM taken into account is given by

$$I_p'(t) = \int dt' I_p(t-t')\Pi(t_{\rm walkoff}\colon t') \tag{26}$$

where $I_p(t) = e^{-t^2/t_{\rm probe}^2}$ is the temporal profile of the probe pulses and $\Pi(t_{\rm walkoff}\colon t)$ is the unit pulse function, given as

$$\Pi(t_{\rm walkoff}\colon t) = \begin{cases} 1, & -t_{\rm walkoff}/2 < t < t_{\rm walkoff}/2 \\ 0, & \text{otherwise.} \end{cases} \tag{27}$$

The measured THz waveform $E_{\rm meas}(t)$ can be calculated using the convolution integral of

$$E_{\rm meas}(t) = \int dt' E_{\rm rad}(t') I_p'(t-t'). \tag{28}$$

In the calculation, we used $t_{\rm probe} = 0.2$ ps and $t_{\rm walkoff} = 0.4$ ps.

III. Experimental Setup

The experimental setup for the narrow-band THz generation through multiple-pulse excitation is shown in Fig. 2. An amplified Ti : sapphire laser system produces 130-fs 0.7-mJ pulses at 800 nm with a repetition rate of 1 kHz. We carefully eliminated the prepulses preceding the main amplified pulse by >1 ns by placing a Pockel's cell after the amplifier. This was necessary since even very small prepulses could affect the saturation properties of the emitter. Roughly 90% of this beam is input into a novel hyper-Michelson interferometer [20], which is used to produce a train of equal-amplitude pulses separated by 3.3 ps, corresponding to a repetition rate of 300 GHz. Fig. 3 shows the hyper-Michelson interferometer

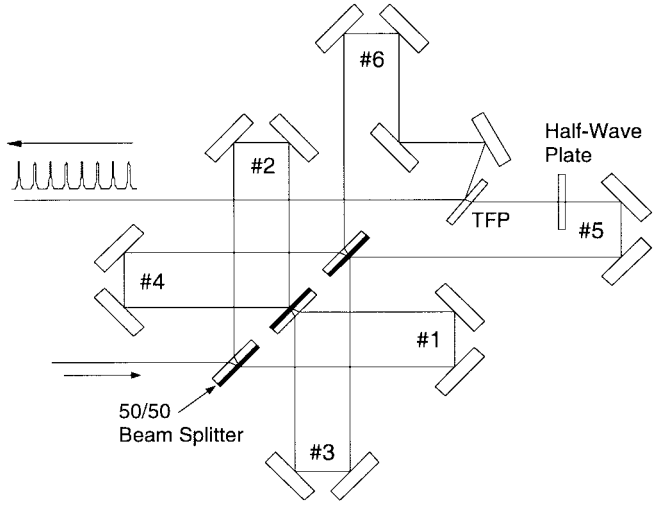

Fig. 3. The hyper-Michelson interferometric pulseshaper used in this experiment. The version shown here and used in the experiments can generate a maximum of 8 pulses. TFP: thin-film polarizer; #1–6 are pairs of mirrors mounted on the micrometer translational stages.

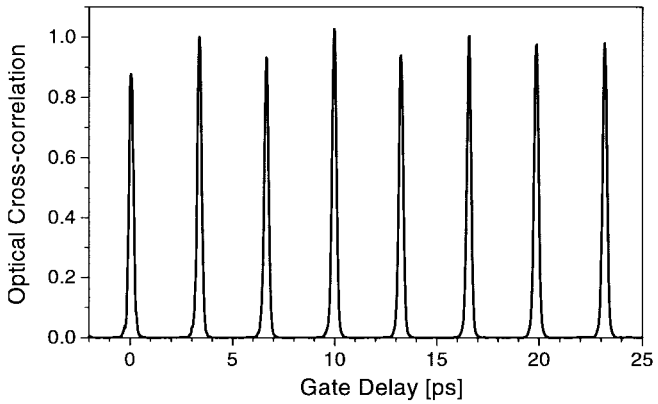

Fig. 4. Cross correlation in a 500-μm KDP crystal of the 8-pulse optical pulse output from the hyper-Michelson interferometer with a single optical gate pulse.

used in this work, which can generate 2–8 pulses. We chose to generate pulse sequences after the amplification of the optical pulses in the regenerative amplifier in order to avoid crosstalk between the adjacent pulses during amplification [21]. A typical cross correlation of an 8-pulse optical pulse output from this interferometer with the unshaped reference gate pulse is shown in Fig. 4. The optical pulse train is lightly focused to a 4-mm-diameter spot and is incident on a 5-mm-gap photoconductive emitter biased at 3 kV/cm. E-O sampling with a 1-mm-thick $\langle 1\bar{1}0 \rangle$ ZnTe crystal was used to detect the THz radiation. The THz electric field is mapped out temporally by scanning the time delay between the probe pulse and the THz pulse train using a computer-controlled stepper motor stage.

We studied four PC emitters made on SI-GaAs and LT-GaAs [13]. The photoconductors consisted of a 1-mm-thick SI-GaAs sample and three samples with a 2.8-μm-thick LT-GaAs layer grown on a 0.6-mm-thick SI-GaAs substrate. The LT-GaAs layers were grown at 280 °C by molecular beam epitaxy and subsequently annealed for 30 s at 575 °C, 600 °C, and 625 °C.

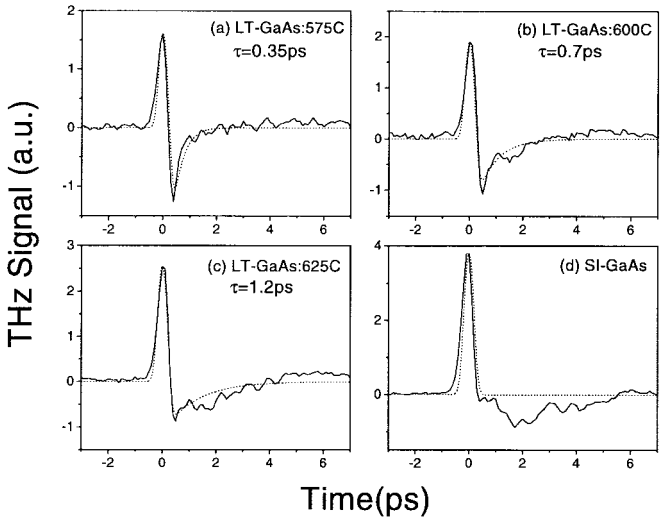

Fig. 5. THz radiation waveforms from LT-GaAs and SI-GaAs emitters with the excitation by low optical fluence single pulses. The solid lines represent the measured waveforms and the dashed lines represent the calculated waveforms. Emitter material: (a) LT-GaAs annealed at 575 °C, (b) LT-GaAs annealed at 600 °C, (c) LT-GaAs annealed at 625 °C, and (d) SI-GaAs.

For the SI-GaAs sample, the carrier lifetime is >100 ps, while for the LT-GaAs samples, the lifetimes are all <10 ps. We used a thick layer of LT-GaAs (2.8 μm) to reduce the absorption of the light in the substrate and subsequent contributions of the carriers generated in the substrate to the THz signal.

IV. Results

A. Single Pulse Excitation

Fig. 5 shows the THz waveforms from four emitters excited by single pulses of low optical excitation fluence. The dotted lines are the calculated waveforms. The lifetime of the photogenerated carriers used in the calculation is given in each figure. Because of the very low excitation fluence, the saturation effect is almost negligible, and the carrier lifetimes of the photoconductors were the only adjustable parameters in this fit. From the three waveforms from LT-GaAs emitters (a–c), we can clearly identify the transition from nearly symmetrical bipolar radiation to asymmetrically bipolar or almost unipolar radiation. This is a direct consequence of the different carrier lifetimes of LT-GaAs layers annealed at different temperatures. The SI-GaAs emitter has almost unipolar waveforms. The slight negative feature in the waveforms from the SI-GaAs emitter after the main peak is not understood at this time. Some of us recently reported on the comparison between the THz waveforms measured by E-O and PC-sampling techniques using the same LT-GaAs photoconductors as detectors [22]. In that research, we used a 1.3-ps carrier lifetime as a fitting parameter to model the PC detector fabricated on LT-GaAs annealed at 600 °C which is substantially different from the 0.7 ps used as a fitting parameter here. This discrepancy might be related to the presence of several different lifetimes in the semiconductor and the possibility of our detecting different lifetimes depending on whether we use the material as an emitter or as a detector. To independently determine the

TABLE I
CARRIER LIFETIMES OF LT-GaAs MEASURED BY OPTICAL PUMP-PROBE MEASUREMENTS AND ELECTRICAL LIFETIME MEASUREMENTS USING SLIDING CONTACT

Annealing Temp.(°C)	Pump/probe at 855nm	Pump/probe at 810nm	sliding contacts
575	0.4ps	0.4ps	—
600	0.7ps	1.1ps	1.1ps
625	1.0ps	1.6ps	—

carrier lifetime, we performed optical pump-probe differential reflection measurements and electrical lifetime measurements using sliding contact excitation [23]. The results of these measurements are summarized in Table I. The optical pump-probe measurements at 855 and 810 nm measured different lifetimes, and, for 600 °C annealed LT-GaAs, they are close to the value used here for the emitter and the value used to model the PC detector, respectively. The sliding contact measurements at 810 and 855 nm produced lifetimes close to the one measured by the optical pump probe at 810 nm. Despite the range of lifetimes obtained from these different measurements, we can say that the lifetimes used to fit Fig. 5 are within the range of values estimated via these techniques. We also note that exact fitting of the single-pulse data of Fig. 5 is not essential for our multiple-pulse experiments discussed below.

Fig. 6 shows the measured THz waveforms emitted from the SI-GaAs emitter and LT-GaAs emitter annealed at 600 °C under single-pulse excitation. Excitation fluences of 5 μJ/cm^2 [Fig. 6(a) and (c)], and 500 μJ/cm^2 [Fig. 6(b) and (d)] are shown here. We can observe several features. While the waveforms from the SI-GaAs emitter did not change much at different excitation fluences, the waveforms from the LT-GaAs emitter changed dramatically when the fluence was increased from 5 to 500 μJ/cm^2. We can clearly observe that the negative peak, which is as high and fast as the positive peak in the low fluence excitation case as shown in Fig. 6(a), becomes very broad and weak. This can be explained by the saturation effect. The positive and negative peaks come from the rising and falling edges of the current profile, respectively. When the excitation fluence is small, i.e., when the emitter is not saturated, the current follows the temporal profile of the carrier concentration. When the carrier concentration dies out after a short lifetime, the current does too, which generates a strong negative peak. When the emitter is excited by high fluence pulses, the emitter is driven into the saturation regime. In deep saturation, the current is no longer sensitive to the carrier concentration or conductivity and the current cannot decay quickly, even when the carrier concentration does. This slow decay of the current at high fluence leads to the smaller and extended negative feature. Furthermore, with high fluence excitation, a lot of carriers are generated in the substrate, and the presence of the large population of long-lifetime carriers affects the waveforms.

With low fluence excitation, the THz radiation from the SI-GaAs emitter is stronger (positive peak = 3.7) than the THz from the LT-GaAs emitter (positive peak = 1.6). But, at

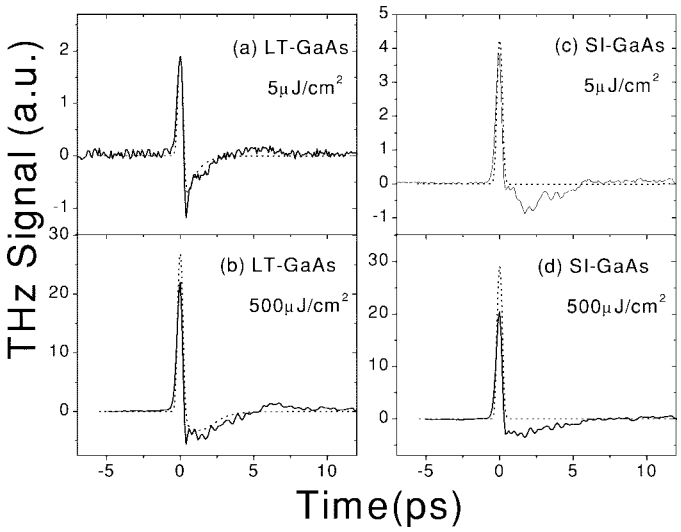

Fig. 6. THz radiation waveforms from (a), (b) a LT-GaAs emitter (annealed at 600 °C) and (b), (d) a SI-GaAs emitter. The emitters were excited by (a), (c) low fluence (5 μJ/cm^2) and (b), (d) high fluence (500 μJ/cm^2) excitation. The solid lines represent the measured waveforms and the dashed lines represent the calculated waveforms.

the high fluence, THz emission from LT-GaAs is comparable to or slightly stronger than the emission from SI-GaAs. This is because for low fluence excitation the mobility of the photoconductor determines the strength of the THz radiation, while at the high fluence they saturate at the same strength determined by the bias value. The dashed lines in Fig. 6 show the calculated THz waveforms from the SI-GaAs emitter and the LT-GaAs emitter with the corresponding excitation conditions used in the experiments. Throughout this paper, the linear absorption coefficient ($\alpha_0 = 1.25/\mu$m) was used. The amplitude of the calculated waveforms was normalized so that the measured and calculated waveforms have the same peak intensity for low fluence excitation of LT-GaAs [Fig. 6(a)]. We observed good agreement in the amplitude between the corresponding measured and calculated waveforms in Fig. 6. Again, the negative features in the waveforms from SI-GaAs cannot be explained. The waveform measured with high fluence excitation of LT-GaAs generated a waveform very close to the one predicted by calculation.

With single-pulse excitation, little improvement was possible in obtaining high-power THz radiation, even when we used short-lifetime material, because all were subject to the same saturation limits from the carrier lifetime being much longer than the pulse duration. (Even with the carrier lifetime much shorter than the pulse duration, one cannot get enhancement because then the amount of current itself will be reduced.)

B. Two Pump-Pulse Experiments

In order to observe the duration of the saturation effect directly, we performed two pump-pulse experiments [8] on the LT-GaAs and SI-GaAs emitters. We used two equal fluence optical pump pulses to excite the emitters and scanned the spacing between the two pump pulses, while only one of the pump pulses was mechanically chopped. The probe pulse delay was set such that we measured the peak THz signal

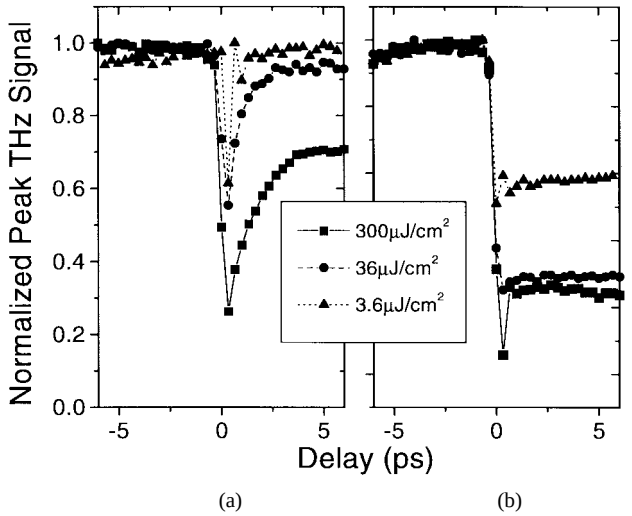

Fig. 7. Results of two pump-pulse THz emission experiments where the peak amplitude of the THz pulse excited by the second pump pulse is plotted versus interpulse separation for (a) a LT-GaAs emitter annealed at 600° and (b) a SI-GaAs emitter.

from the chopped excitation beam. Fig. 7 shows the results of the two pump-pulse experiments on (a) SI-GaAs and (b) LT-GaAs emitters. The LT-GaAs emitter was annealed at 600 °C. The results for optical fluence of 300, 36, and 3.6 μJ/cm^2 for each pump pulse are shown and all results are individually normalized. As expected from the results of [8], for the SI-GaAs emitter, the radiation from the chopped pump pulse is reduced from the value before the arrival of the unchopped pump (negative time delay in the figure) and does not recover at all. Some sharp features around zero time delay seem to be a coherent artifact arising from the interaction of two pump pulses when they overlap in time [24]. We observe that the saturation effect in SI-GaAs is quite dramatic even with low fluence excitation. In the single-pulse excitation experiment, saturation effects are very weak for excitation fluences below a few μJ/cm^2. The difference arises because the far-field radiation is generated predominantly during the rising edge of the current profile in the SI-GaAs. Therefore, in the single-pulse excitation case, the peak of the THz field does not correspond to the near maximum of the carrier concentration, and the THz emission process suffers less from saturation. But, in the two-pump-pulse (or multiple-pulse) experiment, the carrier population generated by the first pulse has not decayed when the second pulse arrives. Therefore, the THz generation process from the second excitation pulse sees the entire carrier concentration from the first pulse and experiences severe saturation.

In contrast to the SI-GaAs emitter, the LT-GaAs emitter shows very different features, including a very fast recovery. Once again, the sharp feature which is seen very clearly for 30 μJ/cm^2 excitation fluence case seems to be a coherent artifact. Because of this, it is difficult to determine the recovery time of the LT-GaAs from this low fluence excitation data. However, the recovery looks complete after 1.3 ps. The higher fluence excitation results show somewhat slower and incomplete recovery which becomes worse with increasing fluence. This feature seems to be from absorption of the pump

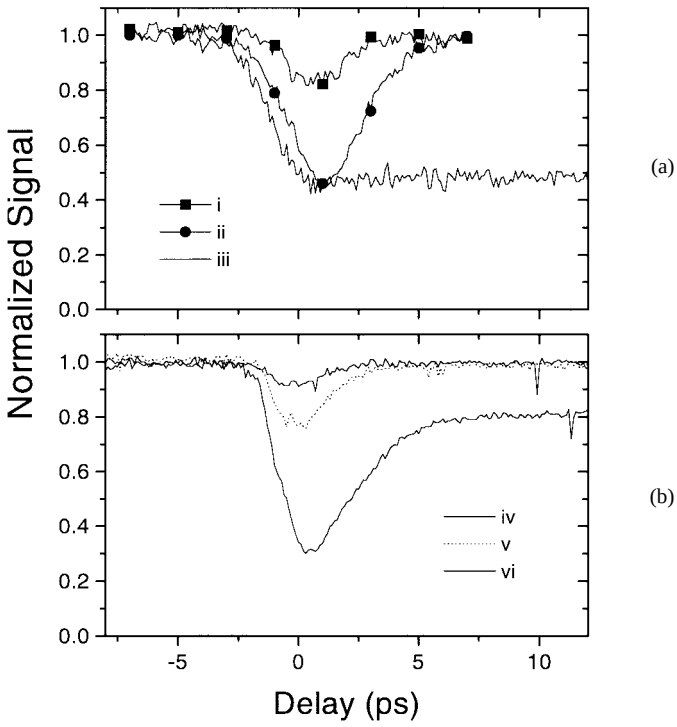

Fig. 8. Optical pump and THz probe experiments on LT-GaAs samples. (a) 1-μm-thick LT-GaAs: (i) 60-μJ/cm^2 pump fluence, substrate removed, (ii) 440-μJ/cm^2 pump fluence, substrate removed, and (iii) 80-μJ/cm^2 pump fluence, with substrate (b) 2.8-μm-thick LT-GaAs with substrate: (iv) 10-μJ/cm^2 pump fluence, (v) 30-μJ/cm^2 pump fluence, and (vi) 220-μJ/cm^2 pump fluence.

light in the substrate. One might think of the possibility of the saturation of traps in the LT-GaAs layer [25]. The fast removal of the carriers from the conduction band in the LT-GaAs is due to the traps induced by excessive arsenic in the epitaxial film. But, when the traps remove electrons from the conduction band, the actual recombination of the trapped electrons with the holes occurs on a much longer time scale. Therefore, once the trap is filled with electrons, the trapping of the electrons in the conduction band stops. Although we cannot rule out the possibility of trap saturation, this seems not to be the dominant cause of the incomplete and slow recovery shown here. To confirm this further, we performed optical pump and terahertz probe experiments [26] on the LT-GaAs. The experiments were performed on the same LT-GaAs sample as well as on a 1-μm-thick LT-GaAs film grown under similar conditions. To isolate the effect of the substrate, we repeated the experiments with this 1-μm-thick sample both with and without the substrate. The results are shown in Fig. 8. In the case with the substrate-removed 1-μm-thick sample [Fig. 8(a)-(i) and (ii)], the recovery was complete in the excitation fluence range $\leq$450 μJ/cm^2, while the 1-μm-thick sample with the substrate [Fig. 8(a)-(iii)] showed incomplete recovery even with 80-μJ/cm^2 excitation fluence. The results with a 2.8-μm-thick sample are shown in Fig. 8(b) and it shows incomplete and slow recovery at the higher fluences. When compared with the data from the 1-μm-thick samples, the observed incomplete recovery can be attributed to substrate absorption. There is no evidence of trap saturation effects.

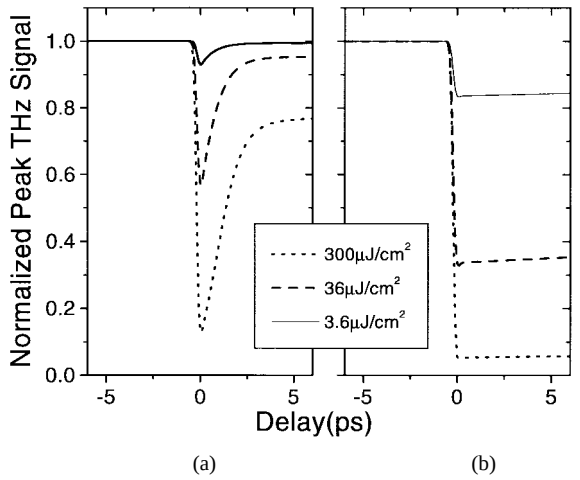

Fig. 9. Simulated results of two pump-pulse THz emission experiments where the peak amplitude of the THz pulse excited by the second pump pulse is plotted versus interpulse separation for a SI-GaAs emitter and a LT-GaAs emitter. (a) LT-GaAs layer on SI-GaAs substrate: $\tau_{r,\,\mathrm{LT}} = 0.7$ ps, $\tau_{r,\,\mathrm{SI}} = 100$ ps. (b) SI-GaAs: $\tau_r = 100$ ps.

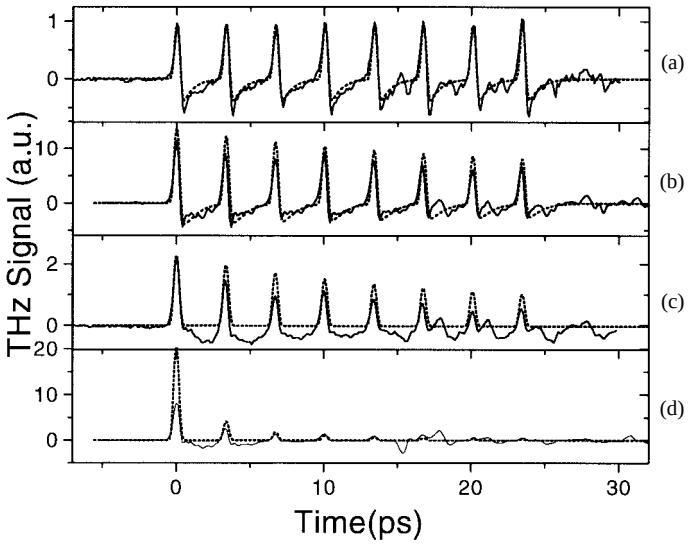

Fig. 10. Measured and calculated THz radiation waveforms from LT- and SI-GaAs emitters excited by 8-pulse sequences. The LT-GaAs was annealed at 600 °C. (a), (b) LT-GaAs emitter. (c), (d) SI-GaAs emitter. (a), (c) Excitation fluence of 20 μJ/cm^2. (b), (d) Excitation fluence of 500 μJ/cm^2.

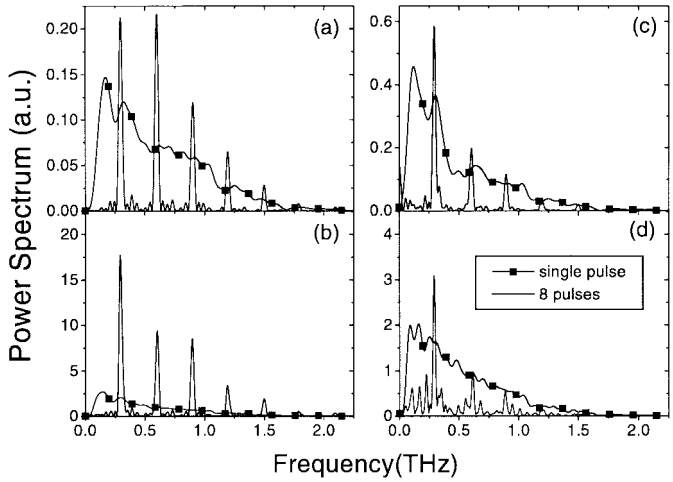

Fig. 11. Power spectral density of THz radiation excited by a single pulse and an 8-pulse sequence. (a), (b) LT-GaAs emitter (annealed at 600 °C). (c), (d) SI-GaAs emitter. (a), (c) Low integrated excitation fluence (20 μJ/cm^2). (b), (d) High integrated excitation fluence (500 μJ/cm^2).

We performed simulations of the two pump-pulse experiments to verify our understanding of the saturation. Because of the nature of the pump scheme where only one of the two pump pulses was chopped, the simulation procedure was modified a little in order to simulate the detection of the THz radiation from the second excitation pulse only. First, we calculated the reference THz waveform with a single excitation pulse. Then, we repeated the calculations with two pump pulses, and the simulated THz waveforms corresponding to our experiment were obtained by subtracting the reference THz waveform from the calculated two-pump-pulse excited waveform. Fig. 9 shows the result of the simulation. For this simulation, the electron mobilities of LT-GaAs and SI-GaAs were assumed to be 1500 and 3000 cm^2/V·s, respectively. The carrier lifetime was 0.7 ps for the LT-GaAs layer and 100 ps for the SI-GaAs layer. We observe a qualitative agreement between the corresponding curves in Figs. 7 and 9. We observe that the combined response from the LT-GaAs layer and the SI-GaAs substrate is slowed down when excited by very high fluence, and the emission does not recover to its original value after a long time. This again confirms the importance of the role of the substrate absorption when we design LT-GaAs emitters for high optical excitation fluence operation.

C. Narrow-Band THz Generation Using Multiple-Pulse Excitation

Fig. 10 shows the representative THz waveforms for excitation by an 8-pulse sequence from LT-GaAs emitters annealed at 600 °C [(a), (b)] and SI-GaAs [(c), (d)] emitters. Fig. 10(a) and (c) show the case of 20-μJ/cm^2 integrated optical excitation fluence and Fig. 10(b) and (d) are of 500-μJ/cm^2 integrated fluence. The small peaks which appear at around 15, 19, and 22 ps are from reflections. The corresponding calculated waveforms are plotted as dotted lines in Fig. 10. The same parameters were used as before. As observed in Fig. 10(a), when the optical excitation fluence is low, the THz pulse trains from the LT-GaAs are just the linear combination of the THz waveform by single pulse excitation. This is exactly expected when there is no saturation. On the other hand, Fig. 10(c) shows that the THz pulse train from SI-GaAs suffers from saturation even with low fluence excitation which is evidenced by the decreasing amplitude of the peaks. When the excitation fluence is increased to 500 μJ/cm^2, the LT-GaAs emitter also begin to show some sign of the saturation [Fig. 10(b)]. This saturation is, as we discussed in Section IV-B, from the photocarrier generation in the SI-GaAs substrate. But, even in this case, the last pulse in the train retains more than 60% of the peak amplitude than the first one.

Fig. 11 shows power spectra of the THz waveforms from the LT-GaAs [(a), (b)] and the SI-GaAs [(c), (d)] samples excited by either a single pulse or an 8-pulse sequence. Fig. 11(a) and (c) show 20-μJ/cm^2 integrated fluence while (b) and (d) show the fluence of 500 μJ/cm^2. The fluence of 20 μJ/cm^2

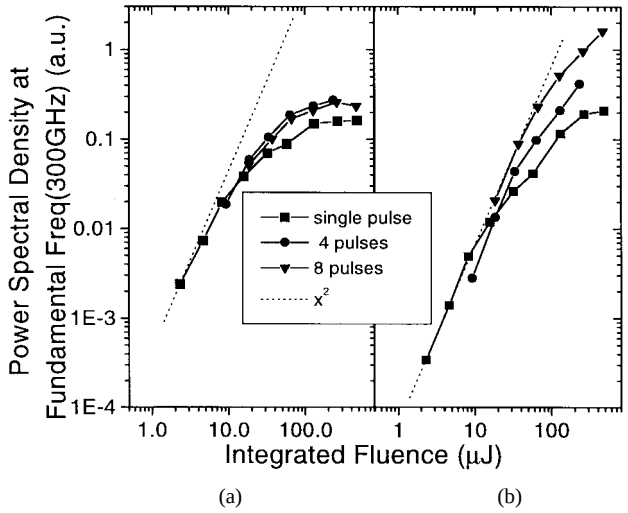

Fig. 12. Power spectral density of THz radiation at the fundamental frequency of 0.3 THz versus optical fluence. (a) SI-GaAs emitter and (b) LT-GaAs emitter (600 °C annealed).

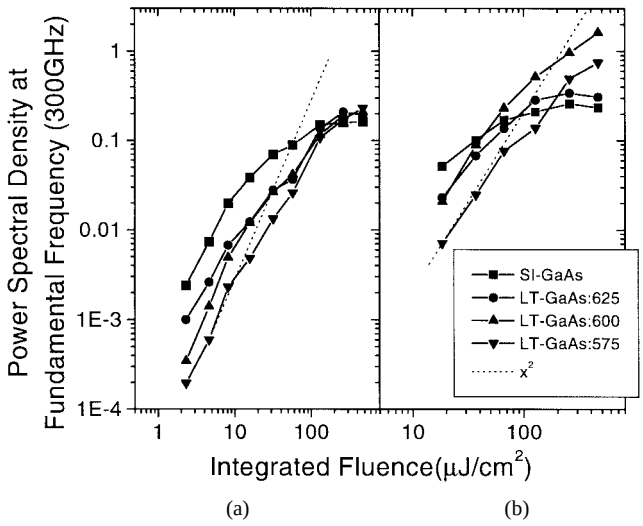

Fig. 13. Power spectral density of THz radiation at the fundamental frequency of 0.3 THz versus optical fluence. (a) Single-pulse excitation. (b) Eight-pulse sequence excitation.

was the lowest fluence where both single-pulse and 8-pulse excitation data were taken. We can see that at 20 μJ/cm^2 excitation fluence, the emitters are already experiencing slight saturation in single-pulse excitation case, because the peaks of the 8 pulse excited THz spectrum go higher than the spectral density obtained from the single-pulse excitation waveforms. In Fig. 11(c), we clearly observe high-power narrow-band THz radiation achieved by using multiple-pulse excitation.

In Fig. 12, the power spectral density at the fundamental frequency ($f = 1/T = 300$ GHz) of the THz waveforms from (a) SI-GaAs and (b) LT-GaAs emitters excited by single or multiple pulses are shown. The LT-GaAs sample was annealed at 600 °C. It should be noted again that, in the 8-pulse excitation case, the term "fluence" means integrated fluence over all pulses in the pulse train. The dashed line is to guide the eye and it represents the quadratic fluence dependence of the power spectral density. When the emitter is not saturated, the peak power spectral density is expected to follow this quadrature dependence, because the THz amplitude should be proportional to the current density which is proportional to the optical excitation fluence through the photogenerated carrier density. Judging from the slope of the curve in Fig. 12(a), the SI-GaAs emitter seems to be in slight saturation even with the lowest excitation fluence. This is in agreement with the time domain data shown in Fig. 10. When the fluence is increased, we observe very strong saturation of the THz power for all single- or multiple-pulse excitation cases with the SI-GaAs emitter. The spectral power density data for the LT-GaAs emitter shows different features. In the lowest excitation region, the slope of the curve is almost exactly two. This is in agreement with the time domain data which showed the linear operation of the emitter. Also, when we increased the excitation fluence, multiple-pulse excitation gives stronger THz radiation than single-pulse excitation. The enhancement obtained by using 8–pulse excitation compared to single-pulse excitation is 7.5 for an excitation fluence of 500 μJ/cm^2.

In Fig. 13, the power spectral density at the fundamental frequency of the THz waveforms from SI-GaAs and LT-GaAs emitters excited by (a) a single-pulse or (b) 8 pulses is shown. The dashed lines are guides for eye. When the emitter is excited by a single pulse of low fluence, the THz amplitude is proportional to the mobility and bias electric field. When we look at the low fluence excitation part of Fig. 13, we observe that the SI-GaAs emitter generates the strongest radiation and the LT-GaAs emitter annealed at 575 °C generates the weakest radiation. This is expected because of the reduced mobility of LT-GaAs, especially when annealed at lower temperatures. From this, we can estimate the difference in mobility. Since the current is proportional to the mobility, the factor of 12 difference in THz power translates into a factor of $\sqrt{12} \simeq 3.5$ difference in mobility between the SI-GaAs and the LT-GaAs samples annealed at 575 °C, in rough agreement with the reported value [27]. With high fluence excitation, all the THz radiation power densities converge to a single value determined by the bias. Here, we observe that the high electron mobility of the SI-GaAs photoconductor does not contribute to high THz amplitude when it is limited by saturation. In Fig. 13(b), we find again that at low excitation fluence the high mobility of the SI-GaAs layer has the advantage of generating more THz energy even with 8-pulse excitation. But, when the excitation fluence is increased, this order is reversed and, at the highest fluence used in the experiments, the SI-GaAs emitter generated the least THz power. When comparing LT-GaAs emitters, the LT-GaAs emitter annealed at 600 °C had the best performance. The reason that the 600 °C annealed LT-GaAs had a better performance than the one annealed at 575 °C is the higher mobility of the 600 °C sample. But, it should be noted that none of the curves are in complete saturation in the fluence range used in our experiments, as can be seen from the slopes of the curves. It is possible that when we further increase the fluence the 575 °C annealed sample may have the best performance. Fig. 14 shows the calculated version of Fig. 12. The same set of parameters as in Section IV-B was used for this calculation which corresponds to the emitters on SI-GaAs and LT-GaAs annealed at 600 °C

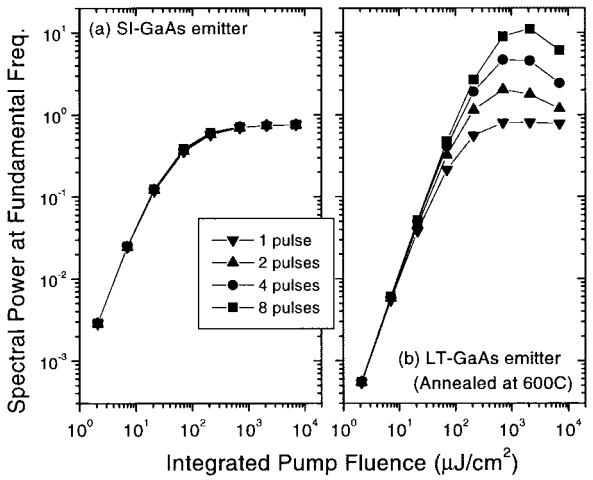

Fig. 14. Calculated power spectral density of THz radiation at the fundamental frequency of 0.3 THz versus optical fluence. (a) SI-GaAs emitter. (b) LT-GaAs emitter (0.7 ps carrier lifetime).

($\mu_{\rm LT} = 1500$ cm^2/V·s, $\mu_{\rm SI} = 3000$ cm^2/V·s, $\tau_{r,\,\rm LT} = 0.7$ ps, and $\tau_{r,\,\rm SI} = 100$ ps). Fig. 14(a) shows that for the SI-GaAs emitter no enhancement can be obtained by using multiple-pulse excitation when the integrated fluence is fixed, while Fig. 14(b) shows large enhancement from the LT-GaAs emitter excited by the multiple-pulse sequence. An interesting note is that the performance of the LT-GaAs emitter becomes poorer above 2-mJ/cm^2 excitation fluence. This derives from the fact that at very high fluence the carriers generated in the substrate dominate the saturation process. Therefore, at the high fluence limit, the performance of the LT-GaAs emitter converges to that of SI-GaAs. This gives the upper bound of excitation energy which can be used to extract more THz energy. From the calculation, we estimate this energy for our LT-GaAs emitter to be between 1 and 5 mJ/cm^2.

In Section II-A, it was shown that when an emitter is in complete saturation, the enhancement in the peak power spectral density which can be obtained by using an N-pulse sequence is a factor of N^2. In this case of 8-pulse excitation, this predicts a factor of 64 enhancement. The reason that we have only a factor of 7.5 enhancement is twofold. When the excitation fluence is very high, the saturation effect from the photogenerated carriers in the substrate plays an important role. Therefore, the assumption of complete recovery between the pulses in the pulse train which was assumed in the theory does not hold. Second, in the theory, we assumed that the emitter is in complete saturation such that the individual pulses in the train can generate the THz radiation of the same strength as the single-pulse excitation which has the same integrated fluence as the whole pulse train. But, in this experiment, it is not the case. In Fig. 13(a), we observe that the THz power density from the 600 °C annealed LT-GaAs emitter by single-pulse excitation at energy fluences of 500 and 60 μJ/cm^2 are different by a factor of $\sim$5. The fluence of 60 μJ/cm^2 is approximately the same fluence as that for the individual pulses in the 500-μJ/cm^2 integrated fluence 8-pulse sequence. Therefore, we know that the individual pulses in that pulse train do not drive the emitter into complete saturation. If we carefully observe the slope of the curve for 600 °C annealed LT-GaAs in Fig. 13, we can find that even a single pulse of 500 μJ/cm^2 cannot drive the system into complete saturation. Therefore, to observe the predicted maximum enhancement of 64, the integrated fluence of the 8-pulse sequence should be larger than $500 \times 8 = 4$ mJ/cm^2.

V. Conclusion

We developed large-aperture photoconductive THz emitters that can generate high-power narrow-band THz radiation. We reduced saturation effects and enhanced the peak power spectral density of the emitted THz radiation by using multiple-pulse excitation of the low-temperature-grown GaAs (LT-GaAs) PC emitters whose carrier lifetime is shorter than the pulse spacing. We have investigated the saturation properties of the biased large-aperture photoconductors excited by trains of amplified femtosecond optical pulses. A direct comparison was made of the saturation properties of SI-GaAs and LT-GaAs emitters with different carrier lifetimes in view of the multiple-pulse excitation. Both numerical calculations based on the radiation screening theory of a large-aperture antenna and the experimental results showed that a large enhancement of the narrow-band THz output under multiple-pulse excitation is possible when the carrier lifetime of the photoconductor is less than the interpulse spacing. When the carrier lifetime was longer than the interpulse spacing, the radiation screening effect from the long-lived current reduced the enhancement. This confirms the near-field nature of the saturation from radiation screening. We also found that the thickness of the short carrier lifetime photoconducting thin film is a very important parameter. If the photoconductor is not thick enough, substantial population of carriers is generated in the long carrier lifetime substrate when the emitter is excited by high fluence pulses, which degrades the THz emission.

References

[1] J. T. Darrow, X.-C. Zhang, D. H. Auston, and J. D. Morse, "Saturation properties of large-aperture photo-conducting antennas," *IEEE J. Quantum Electron.*, vol. 28, pp. 1607–1616, 1992.
[2] D. You, R. R. Jones, P. H. Bucksbaum, and D. R. Dykaar, "Generation of high-power sub-single-cycle 500-fs electromagnetic pulses," *Opt. Lett.*, vol. 18, pp. 290–292, 1993.
[3] E. Budiarto, J. Margolies, S. Jeong, J. Son, and J. Bokor, "High-intensity terahertz pulses at 1-kHz repetition rate," *IEEE J. Quantum Electron.*, vol. 32, pp. 1839–1846, 1996.
[4] J. T. Darrow, X.-C. Zhang, and D. H. Auston, "Power scaling of large-aperture photoconducting antennas," *Appl. Phys. Lett.*, vol. 58, pp. 25–27, 1991.
[5] J. E. Pedersen, V. G. Lyssenko, J. M. Hvam, P. U. Jepsen, S. R. Keiding, C. B. Sorensen, and P. E. Lindelof, "Ultrafast local field dynamics in photoconductive THz antennas," *Appl. Phys. Lett.*, vol. 62, pp. 1265–1267, 1993.
[6] A. J. Taylor, P. K. Benicewicz, and S. M. Young, "Modeling of femtosecond electromagnetic pulses from large-aperture photoconductors," *Opt. Lett.*, vol. 18, pp. 1340–1342, 1993.
[7] P. K. Benicewicz and A. J. Taylor, "Scaling of terahertz radiation from large-aperture biased InP photoconductors," *Opt. Lett.*, vol. 18, pp. 1332–1334, 1993.
[8] A. J. Taylor, G. Rodriguez, and D. Some, "Ultrafast field dynamics in large-aperture photoconductors," *Opt. Lett.*, vol. 22, pp. 715–717, 1997.
[9] Y. Liu, S.-G. Park, and A. M. Weiner, "Enhancement of narrow-band terahertz radiation from photoconducting antennas by optical pulse shaping," *Opt. Lett.*, vol. 21, pp. 1762–1764, 1996.
[10] ——, "Terahertz waveform synthesis via optical pulse shaping," *J. Select. Topics Quantum Electron.*, vol. 2, pp. 709–719, 1996.

[11] A. S. Weling, B. B. Hu, N. M. Froberg, and D. H. Auston, "Generation of tunable narrow-band THz radiation from large aperture photoconducting antennas," *Appl. Phys. Lett.*, vol. 64, pp. 137–139, 1994.
[12] C. W. Siders, J. L. W. Siders, A. J. Taylor, S.-G. Park, M. R. Melloch, and A. M. Weiner, "Generation and characterization of terahertz pulse trains from biased, large-aperture photoconductors," *Opt. Lett.*, vol. 24, pp. 241–243, 1999.
[13] M. R. Melloch, D. D. Nolte, J. M. Woodall, J. C. P. Chang, D. B. Janes, and E. S. Harmon, "Molecular beam epitaxy of nonstoichiometric semiconductors and multiphase material systems," *Crit. Rev. Solid State Mater. Sci.*, vol. 21, pp. 189–263, 1996.
[14] S. Gupta, Y. Frankel, J. A. Valdmanis, J. F. Whitaker, G. A. Mourou, F. W. Smith, and A. R. Calawa, "Subpicosecond carrier lifetime in GaAs grown by molecular beam epitaxy at low temperatures," *Appl. Phys.*, vol. 59, pp. 3276–3278, 1991.
[15] W. Sha, J.-K. Rhee, T. B. Norris, and W. J. Schaff, "Transient carrier and field dynamics in quantum-well parallel transport: From the ballistic to the quasiequilibrium regime," *IEEE J. Quantum Electron.*, vol. 28, pp. 2445–2455, 1992.
[16] P. K. Benicewicz, J. P. Roberts, and A. J. Taylor, "Scaling of terahertz radiation from large-aperture biased photoconductors," *J. Opt. Soc. Amer. B*, vol. 11, pp. 2533–2546, 1994.
[17] G. Rodriguez and A. J. Taylor, "Screening of the bias field in terahertz generation from photoconductors," *Opt. Lett.*, vol. 21, pp. 1046–1048, 1996.
[18] S. M. Sze, *Physics of Semiconductor Devices*, 2nd ed. New York: Wiley, 1981.
[19] Q. Wu and X.-C. Zhang, "Free-space electro-optic sampling of terahertz beams," *Appl. Phys. Lett.*, vol. 67, pp. 3523–3525, 1995.
[20] C. W. Siders, J. L. W. Siders, A. J. Taylor, S.-G. Park, and A. M. Weiner, "Efficient high-energy pulse train generation using a 2^n-pulse Michelson interferometer," *Appl. Opt.*, vol. 18, pp. 1340–1342, 1998.
[21] X. Liu, R. Wagner, A. Maksimchuk, E. Goodman, J. Workman, D. Umstadter, and A. Migus, "Nonlinear temporal diffraction and frequency shifts resulting from pulse shaping in chirped-pulse amplification system," *Opt. Lett.*, vol. 20, pp. 1163–1165, 1995.
[22] S.-G. Park, M. R. Melloch, and A. M. Weiner, "Comparison of terahertz waveforms measured by electro-optic and photoconductive sampling," *Appl. Phys. Lett.*, vol. 73, pp. 3184–3186, 1998.
[23] D. R. Grischkowsky, M. B. Ketchen, C.-C. Chi, I. I. N. Duling, N. J. Halas, J.-M. Halbout, and P. G. May, "Capacitance free generation and detection of subpicosecond electrical pulses on coplanar transmission lines," *IEEE J. Quantum Electron.*, vol. 24, pp. 221–225, 1988.
[24] E. P. Ippen and C. V. Shank, "Techniques for measurement," in *Ultrashort Light Pulses.* Berlin, Germany: Springer-Verlag, 1984, pp. 83–122.
[25] U. Siegner, R. Fluck, G. Zhang, and U. Keller, "Ultrafast high-intensity nonlinear absorption dynamics in low-temperature grown gallium arsenide," *Appl. Phys. Lett.*, vol. 69, pp. 2566–2568, 1996.
[26] S. S. Prabhu, S. E. Ralph, M. R. Melloch, and E. S. Harmon, "Carrier dynamics of low-temperature-grown GaAs observed via THz spectroscopy," *Appl. Phys. Lett.*, vol. 70, pp. 2419–2421, 1997.
[27] A. Krotkus, S. Marcinkevicius, J. Jasinski, M. Kaminska, H. H. Tan, and C. Jagadish, "Picosecond carrier lifetime in GaAs implanted with high doses of As ions: An alternative material to low-temperature GaAs for optoelectronic applications," *Appl. Phys. Lett.*, vol. 66, pp. 3304–3306, 1995.

Sang-Gyu Park (M'99) was born in Seoul, Korea, in 1967. He received the B.S. and M.S. degrees in electronics engineering from Seoul National University, Korea, in 1990 and 1992, respectively, and the Ph.D. degree in electrical engineering from Purdue University, West Lafayette, IN, in 1998. His doctoral dissertation dealt with the generation and detection of coherent terahertz radiation.

He joined AT&T Labs–Research, Red Bank, NJ, in December 1998, where he is working on high-speed optical fiber communication systems. His research interests include ultrafast optics, terahertz radiation, and optical fiber communications.

A. M. Weiner (S'84–M'84–SM'91–F'95) was born in Boston, MA, in 1958. He received the Sc.D. degree in electrical engineering from the Massachusetts Institute of Technology (MIT), Cambridge, in 1984. His dissertation dealt with femtosecond pulse compression (including generation of the shortest optical pulses reported up to that time) and measurement of femtosecond dephasing in condensed matter.

From 1979 to 1984, he was a Fannie and John Hertz Foundation Graduate Fellow at MIT. In 1984, he joined Bellcore, where he conducted research on ultrafast optics, including shaping of ultrashort pulses, nonlinear optics and switching in fibers, and spectral holography. In 1989, he became Manager of the Ultrafast Optics and Optical Signal Processing Research District. He assumed his current position as Professor of Electrical and Computer Engineering at Purdue University, West Lafayette, IN, in October 1992. Since August 1996, he has also been serving as Director of Graduate Admissions for the School of Electrical and Computer Engineering. His current research interests center on holography of ultrashort pulses, high-speed optical communications, applications of pulse shaping to femtosecond spectroscopy and nonlinear optics, and optical imaging in scattering media. He has published approximately 80 journal articles in the area of ultrafast laser optics and fiber communications and has been author or co-author of over 150 conference papers in this field. He also holds five U.S. patents and has served on numerous research review panels, professional society award committees, and conference program committees. He has served as Associate Editor for *Optics Letters*.

Prof. Weiner is a fellow of the Optical Society of America. He was awarded the Adolph Lomb Medal of the Optical Society of America for pioneering contributions to the field of optics made before the age of thirty. He was also awarded the 1997 Curtis McGraw Research Award of the American Society of Engineering Education and the 1997 International Commission on Optics Prize. He also received the 1984 Hertz Foundation Doctoral Thesis Prize while at MIT. He was Co-Chair of the 1996 and 1998 Conference on Lasers and Electro-optics and Chair of the 1999 Gordon Conference on Nonlinear Optics and Lasers. In 1988–1989, he served as a IEEE Lasers and Electro-optics Society (LEOS) Traveling Lecturer. In addition, he has served as Associate Editor for the IEEE JOURNAL OF QUANTUM ELECTRONICS and IEEE PHOTONICS TECHNOLOGY LETTERS.

Michael R. Melloch (S'76–M'76–SM'91–F'99) received the B.S.E.E., M.S.E.E., and Ph.D. degrees from Purdue University, West Lafayette, IN, in 1975, 1976, and 1981, respectively.

From June 1976 to August 1978, he was a Design Engineer at Intel Corporation, where he worked in the 8275, a CRT controller chip, the 8748, the first single-chip microcomputer, and was co-designer of the 8051, a second-generation single-chip microcomputer. In February 1982, he joined the Central Research Laboratories, Texas Instruments, as a Member of the Technical Staff. At Texas Instruments, his research interests centered around GaAs surface acoustic wave devices. In August 1984, he joined the School of Electrical Engineering, Purdue University, as an Assistant Professor and is presently Full Professor and former Assistant Dean of Engineering. He has co-authored 300 conference lectures, 250 technical papers, 4 book chapters, and holds of 5 U.S. patents. His current research interests are molecular beam epitaxy, optoelectronics, and SiC processing and devices. He has served as a Symposium Co-Organizer for the 1993 and 1999 Spring Meetings of the Material Research Society, the Program Chair for the 1994 North American Conference on Molecular Beam Epitaxy, Co-Organizer of the Eighth International Conference on Superlattices, Microstructures, and Microdevices, Associate Program Chair for the 1997 International Symposium on Compound Semiconductors, and Program Chair of the 1998 and 1999 Electronic Materials Conferences. In 1993, he was elected to the Electronic Materials Committee of the Minerals, Metals & Materials Society and has served as Secretary (1995–1997) and Vice-Chair (1997–1999). He has been a Guest Editor for six journal special issues.

Prof. Melloch is a fellow of the American Physical Society and a member of the American Vacuum Society, the Minerals, Metals & Materials Society, and the Optical Society of America.

Craig W. Siders, for biography, see p. 440 of the April issue of this JOURNAL.

Jennifer L. W. Siders, for biography, see p. 440 of the April issue of this JOURNAL.

Antoinette J. Taylor, for biography, see p. 440 of the April issue of this JOURNAL.